Evaluation of Multiaxial Low Cycle Fatigue Life under Non-proportional Loading

Takamoto ITOH[*, 1] and Masao SAKANE[*, 2]

[*] Department of Mechanical Engineering, Faculty of Science and Engineering,
Ritsumeikan University, 1-1-1, Nojihigashi, Kusatsu-shi, Shiga 525-8577, Japan
[1] E-mail: itohtaka@fc.ritsumei.ac.jp, [2] E-mail: sakanem@se.ritsumei.ac.jp

ABSTRACT. *A simple and clear method of evaluating stress and strain ranges under non-proportional multiaxial loading where principal directions of stress and strain are changed during a cycle is needed for assessing multiaxial fatigue. This paper presents a simple method of determining the principal stress and strain ranges and the severity of non-proportional loading with defining the rotation angles of the maximum principal stress and strain in a three dimensional stress and strain space. This study also discusses properties of multiaxial low cycle fatigue lives for various materials fatigued under non-proportional loadings and shows an applicability of a parameter proposed by author for multiaxial low cycle fatigue life evaluation.*

Keywords: Low cycle fatigue, Multiaxial loading, Non-proportional loading, Life prediction, Design criteria

INTRODUCTION

Most design codes use equivalent values to express the intensity of multiaxial stress or strain, like von Mises or Tresca equivalent stress and strain, and fatigue lives are usually estimated using equivalent values under multiaxial stress and strain states. The equivalent value means a scalar parameter that expresses intensity of a physical phenomenon in multiaxial stress states and should be reduced to be a uniaxial value in uniaxial stress state. Most widely used equivalent parameters are the von Mises and the Tresca equivalent stresses and strains. The von Mises equivalent stress physically expresses the intensity of shear strain energy and the Tresca equivalent stress that of the maximum shear stress. For example, ASME Section III, Division 1 NH [1] uses the von Mises equivalent strain and ASME Section VIII, Division 3 [2] the maximum shear stress.

However, the von Mises equivalent stress and strain have no negative values so that they have a difficulty of expressing stress and strain ranges. The Tresca equivalent stress and strain have negative values but they also have a difficulty to put a sign to the shear stress and strain under multiaxial loading. Especially, in non-proportional loading where the principal stress and strain change their directions, giving a sign to them

becomes more difficult. A simple and clear method of calculating stress and strain ranges is needed for describing multiaxial fatigue.

Multiaxial low cycle fatigue (LCF) lives are reduced under strain controlled non-proportional loading accompanied by additional cyclic hardening compared with proportional loading [3-8] and an appropriate design method of evaluating the non-proportional fatigue life is needed for a reliable design and maintenance of structural components. Classical models particularly applicable in multiaxial fatigue life evaluation under proportional loadings lead to overestimate the lives under non-proportional loadings. For life evaluation under non-proportional loading, commonly proposed models are critical plane approaches that consider specific plane applied the critical damage, such as a Simith-Watoson-Topper [11] and a Fatemi-Socie [12] models. The authors also proposed a strain parameter (Itoh-Sakane model) estimating the non-proportional LCF lives for several materials under various strain histories [6,7,13-16]. This parameter is the strain based model with introducing two parameters, non-proportional factor and material constant. The former one reflects the intensity of non-proportional loading reducing life and the latter one is related to the material dependence for degree of life reduction due to non-proportional loading.

The Simith-Watoson-Topper, the Fatemi-Socie and the Itoh-Sakane models have been demonstrated to be applicable to life evaluation under non-proportional loading using hollow cylinder specimens in a laboratory level. However, these models can be applicable to the life evaluation under limited non-proportional loadings such as the loadings in the plane stress state. Therefore, there is a limit of application of the models to the design of actual components where variation in principal directions of stress and strain vs time is changed 3-dimensionally.

This study proposes a method of evaluating the principal stress and strain ranges and the mean stress and strain, and also shows a method of calculating the non-proportional factor which expresses the severity of non-proportional loading in 3-dimantional (3D) stress and strain space. This study also discusses the material constant, α, used in the strain parameter proposed by author for life estimation under non-proportional multiaxial LCF and presents a simple method to reevaluate α in relation to material constants obtained in a static tension test [16].

DEFINITION OF STRESS AND STRAIN RANGES UNDER NON-PROPORTIONAL LOADING

Definition of stress and strain

Fig. 1 illustrates three principal vectors, $S_i(t)$, applied to a small cube in material at time t in xyz-coordinates (spatial coordinates), where "S" is the symbol denoting either stress "σ" or strain "ε". Thus, $S_i(t)$ are the principal stress vectors for the case of stress and the principal strain vectors for the case of strain. The subscript, i, takes 1, 2 or 3 in descending order of principal stress or strain. The maximum principal vector, $S_1(t)$, is defined as $S_i(t)$ whose absolute value takes maximum one, *i.e.*, $S_1(t)=S_1(t)$ when $S_1(t)$

takes maximum magnitude among $\boldsymbol{S}_i(t)$. The maximum principal value, $\boldsymbol{S}_I(t)$, is defined as the maximum absolute value of $\boldsymbol{S}_i(t)$ as,

$$S_I(t) = |\boldsymbol{S}_I(t)| = \mathrm{Max}\left[\,|\boldsymbol{S}_1(t)|,\;|\boldsymbol{S}_2(t)|,\;|\boldsymbol{S}_3(t)|\,\right] \tag{1}$$

The "Max" denotes taking the larger value from the three in the bracket. The maximum value of $S_I(t)$ during a cycle is defined as the maximum principal value, S_{Imax}, at $t = t_0$ as follows,

$$S_{Imax} = |\boldsymbol{S}_I(t_0)| = \mathrm{Max}\left[\,|\boldsymbol{S}_1(t_0)|,\;|\boldsymbol{S}_2(t_0)|,\;|\boldsymbol{S}_3(t_0)|\,\right] \tag{2}$$

Definition of principal stress and strain directions

Fig. 2 illustrates two angles, $\xi(t)/2$ and $\xi(t)$, to express the rotation or direction change of the maximum principal vector, $\boldsymbol{S}_I(t)$, in the new coordinate system of XYZ, where XYZ-coordinates are the material coordinates taking X-axis in the direction of $\boldsymbol{S}_I(t_0)$ with the other two axes in arbitrary directions. The two angles of $\xi(t)/2$ and $\xi(t)$ are given by

$$\frac{\xi(t)}{2} = \cos^{-1}\left(\frac{\boldsymbol{S}_i(t_0)\,\cdot\,\boldsymbol{S}_i(t)}{|\boldsymbol{S}_i(t_0)|\;|\boldsymbol{S}_i(t)|}\right) \qquad (0 \le \frac{\xi(t)}{2} \le \frac{\pi}{2}) \tag{3}$$

$$\zeta(t) = \tan^{-1}\left(\frac{\boldsymbol{S}_i(t)\cdot\boldsymbol{e}_Z}{\boldsymbol{S}_i(t)\cdot\boldsymbol{e}_Y}\right) \qquad (0 \le \zeta(t) \le 2\pi) \tag{4}$$

where dots in Eqs 3 and 4 denote the inner product and $\boldsymbol{e}_Y$ and $\boldsymbol{e}_Z$ are unit vectors in Y and Z directions, respectively. $\boldsymbol{S}_i(t)$ are the principal vectors of stress or strain used in Eq. 1 and the subscript i takes 1 or 3.
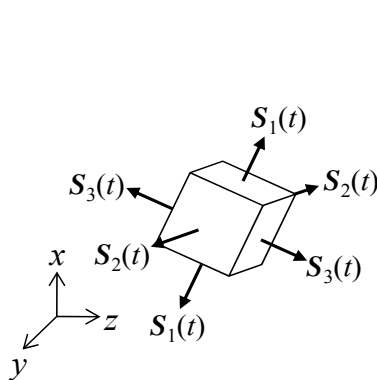

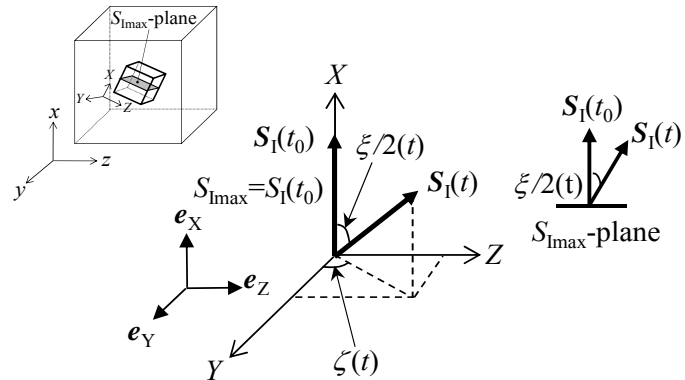Fig. 1. Principal stress and strain in *xyz* coordinates.

Fig. 2. Definition of principal stress and strain directions in *XYZ* coordinates.

The rotation angle of $\xi(t)/2$ expresses the angle between the $S_I(t_0)$ and $S_I(t)$ directions and the deviation angle of $\zeta(t)$ is the angle of $S_I(t)$ direction from the Y-axis in the X-plane.

Definitions of stress and strain in polar figure

Fig. 3 shows the trajectory of $S_I(t)$ in 3D polar figure for a cycle where the radius is taken as the value of $S_I(t)$, and the angles of $\xi(t)$ and $\zeta(t)$ are the angles shown in the figure. A new coordinate system is used in Fig. 3 with the three axes of S_I^1, S_I^2 and S_I^3, where S_I^1-axis directs to the direction of $S_I(t_0)$. The rotation angle of $\xi(t)$ has double magnitude compared with that in the specimen shown in Fig. 2 considering the consistency of the angle between the polar figure and the physical plane presentation. The principal range, ΔS_I, is determined as the maximum projection length of $S_I(t)$ on the S_I^1-axis. The mean value, S_{Imean}, is given as the center of the range. ΔS_I and S_{Imean} are equated as,

$$\Delta S_I = \text{Max}\left[S_{Imax} - \cos\xi(t)\, S_I(t)\right] = S_{Imax} - S_{Imin} \tag{5}$$

$$S_{Imean} = \frac{1}{2}\left(S_{Imax} + S_{Imin}\right) \tag{6}$$

S_{Imin} is the $S_I(t)$ to maximize the value of the bracket in Eq. 5. The sign of S_{Imin} in the figure is set to be positive if it does not cross the S_I^2-S_I^3 plane and the sign negative if it crosses the plane.

The advantage of the definitions of the maximum principal range and mean value above mentioned is that the two are determinable without human judgments for any loading case in 3D stress and strain space. The range and mean value are consistent used in simple loading cases which are discussed in the case studies in the followings. $S_I(t)$ can be replaced by equivalent values of stress or strains, such as the von Mises and the Tresca, in case of necessity from user's requirement.
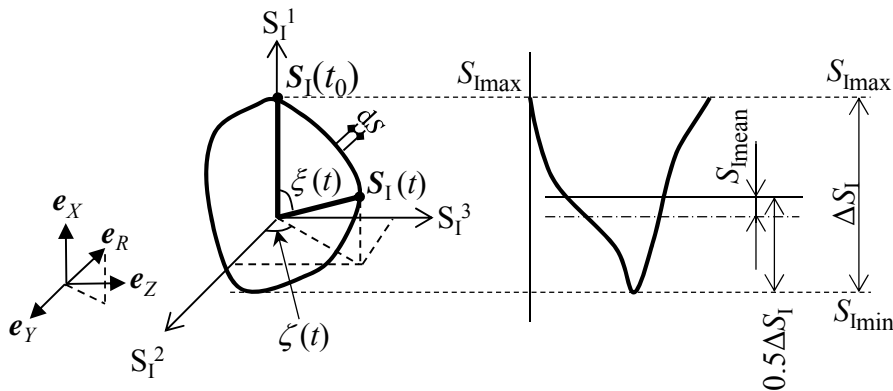

Fig. 3. Definition of principal range and mean principal value.

DEFENITION OF NON-PROPORTIONALITY

The authors proposed the non-proportional strain range expressed in Eq. 7 for correlating LCF lives under non-proportional loading [6,7,13-16].

$$\Delta\varepsilon_{NP} = \left(1 + \alpha\, f_{NP} \right) \Delta\varepsilon_I \tag{7}$$

In the equation, $\Delta\varepsilon_I$ is the principal strain range discussed previously. α is a material constant related to the amount of additional hardening by non-proportional loading, which will be mentioned more detail in sections 4.2 and 4.3.

f_{NP} is the non-proportional factor that expresses the severity of non-proportional loading in the form as,

$$f_{NP} = \frac{b}{T\,\varepsilon_{Imax}} \int_0^T \left(\left| \sin\left(\xi(t)\right) \right|\ \varepsilon_I(t) \right) dt \tag{8}$$

where T is the time for a cycle. b is a constant for making $f_{NP}=1$ in the circular loading on ε-$\gamma/\sqrt{3}$ plot and $b=\pi/2$ [6,7].

This paper presents f'_{NP} in Eq. 9 in 3D expression as an extended form from f_{NP} in 2D shown in Eq. 8.

$$f'_{NP} = \frac{\pi}{2\,S_{Imax}\,L_{path}} \int_C |\boldsymbol{e}_1 \times \boldsymbol{e}_R|\, S_I(t)\, \mathrm{d}s, \qquad L_{path} = \int_C \mathrm{d}s \tag{9}$$

where $\boldsymbol{e}_R$ is a unit vector directing to $S_I(t)$, $\mathrm{d}s$ the infinitesimal trajectory of the loading

Type	1	2	3	4	5	6
Loading path						
f_{NP}	0	0.39	0.10	0.20	0.79	0.79
f'_{NP}	0	0.49	0.12	0.24	0.71	0.71
Type	7	8	9	10	11	12
Loading path						
f_{NP}	0.53	1.06	-	-	-	-
f'_{NP}	0.5	1	0.71	0.98	0.49	1.78

Fig. 4. Comparing f_{NP} and f'_{NP} under several loadings.

path shown in Fig. 3. L_{path} the whole loading path length during a cycle and "×" denotes vector product. The scalars, S_{Imax} and L_{path}, before the integration in Eq. (9) is set to make f'_{NP} unity in the circler loading in 3D polar figure.

Fig. 4 compares the values of f_{NP} with those of f'_{NP} for several loading paths for the case of strain. Small difference in the value between f_{NP} and f'_{NP} is found because of different definition between them. However, f'_{NP} has the advantages applicable to 3D stress and strain conditions.

MULTIAXIAL LOW CYCLE FATIGUE LIVES UNDER NON-PROPORTIONAL LOADING

This chapter shows multiaxial LCF life properties under non-proportional loadings for several materials and shows the applicability of the strain parameter for life estimation, which were studied in authors' previous study [14]

Materials and test procedure
   Test materials employed were 12 metallic materials of which crystal structures (CS) are face-centered cubic structure (FCC) and body-centered cubic structure (BCC) as listedin Table 1 with mechanical properties obtained by static tension test. The specimen usedwas a hollow cylinder specimen with 12 mm outer diameter, 9 mm inner diameter and 7 mm gauge length as shown in Fig. 5.
   Total strain controlled multiaxial LCF tests were conducted under 2 types of strain paths. Figs 6 (a) and (b) show the strain paths on $\varepsilon - \gamma/\sqrt{3}$ plot and the strain waveforms of ε and γ, respectively, where ε and γ are total axial and total shear strains. Case 1 is the

Table 1 List of materials tested and mechanical properties.

Test material		Mechanical property in static tensile test		
Type	CS	Young's modulus E (GPa)	Yield/Proof stress σ_Y (MPa)	Strength σ_B (MPa)
SUS316		197	260	575
SUS304		197	290	750
SUS304 (923K)		150	130	480
SUS310S	FCC	196	215	520
OFHC (Cu)		117	182	240
6061Al		77	253	390
1070Al		70	112	116
SGV410		216	275	470
SUS430		200	263	480
S25C	BCC	200	354	493
S45C		205	445	630
S55C		203	485	695

push-pull test and Case 2 the 90° sinusoidal out-of-phase loading test. The former is the proportional loading test and the latter the non-proportional loading test. Total axial strain ranges ($\Delta\varepsilon$) were set to the same ranges in Case 1 and Case 2 and total axial strain and total shear strain ranges were the same ranges based on von Mises, $\Delta\varepsilon=\Delta\gamma/\sqrt{3}$, in Case 2. Strain rate was 0.1%/sec based on von Mises basis.
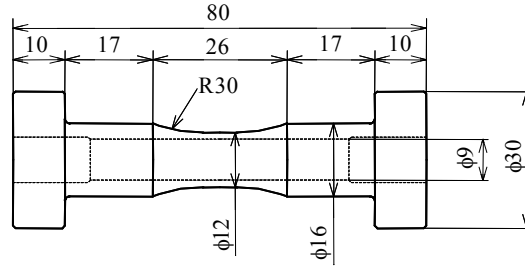

Fig. 5. Shape and dimensions of specimen (mm).

(a) Stain paths on $\varepsilon-\gamma/\sqrt{3}$ plot

(b) Axial and shear strain waveforms
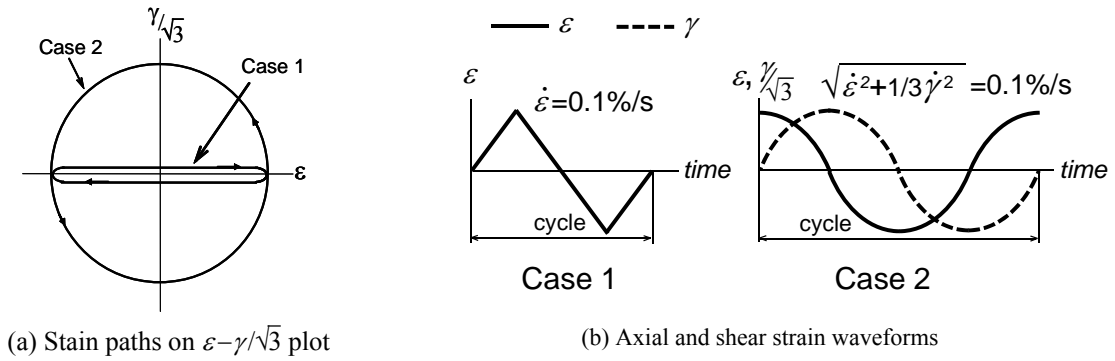
Fig. 6. Strain paths and strain waveforms.

Multiaxial LCF life and additional hardening

To evaluate the material dependency of failure life and cyclic hardening behaviors under non-proportional loading, this section shows the multiaxial LCF test results for SUS316 and SGV410 fatigued in the push-pull and the circle tests using the hollow cylinder specimen (Case 1 and Case 2).

ASME code case [1] defines a strain parameter to express the non-proportional fatigue damage. The strain parameter is originated from the equivalent strain range based on von Mises but it was modified to have a maximum value taking any times C and D along strain paths as shown in Eq. (10).

$$\Delta\varepsilon_{\text{ASME}} = \max\left[\left\{(\varepsilon_C - \varepsilon_D)^2 + \frac{1}{3}(\gamma_C - \gamma_D)^2\right\}^{\frac{1}{2}}\right] \tag{10}$$

where ε_C and γ_C are the axial and shear strains at time C and ε_D and γ_D those at time D to maximize the strain in the bracket. In the tests of Case 1 and Case 2, the values of $\Delta\varepsilon_{ASME}$ correspond with those given by total axial strain range, $\Delta\varepsilon$.

Figs 7 (a) and (b) show failure lives (N_f) of SUS316 and SGV410 correlated by $\Delta\varepsilon$ ($=\Delta\varepsilon_{ASME}$). In the figure, the bold solid line was drawn based on the data of Case 1 and the two thin lines show a factor of 2 band. For SUS316, N_f in Case 2 is about 1/5 of that in Case 1. The similar trend can be seen for SGV410, too. N_f in Case 2 is about 1/5 of that in Case 1. Therefore, the degrees of reduction in failure life due to non-proportional loading between these two steels are almost equivalent.

The overestimation of N_f in Case 2 by the life curve in Case 1 also has been reported and it is known that the reduction in failure life under non-proportional loading is related to the additional hardening due to non-proportional loading depending on material [5,16-19].
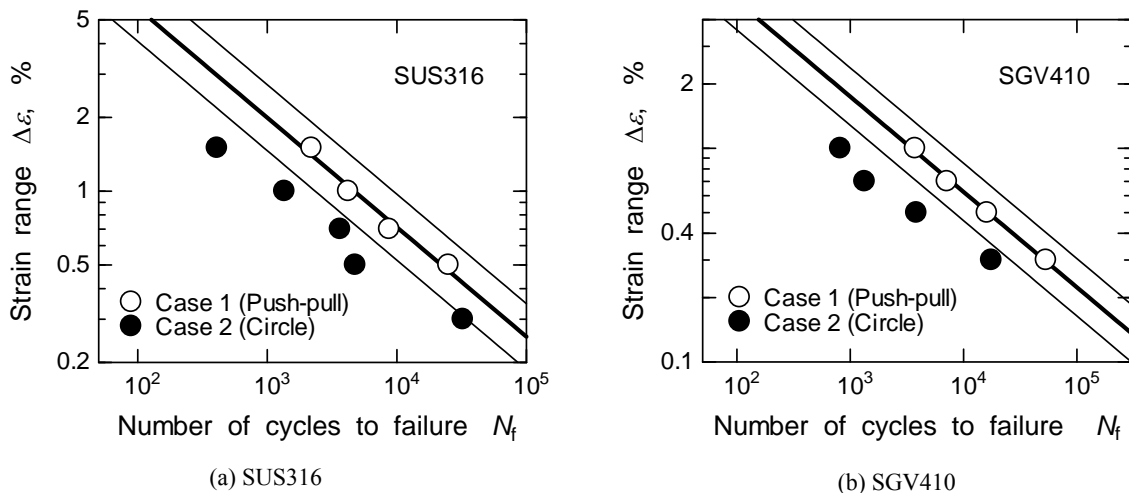

(a) SUS316 (b) SGV410

Fig. 7. Relationship between $\Delta\varepsilon$ and N_f.

Figs 8 (a) and (b) show cyclic stress-strain relations for SUS316 and SGV410 respectively obtained by a multiple step-up test under two strain paths using the hollow cylinder specimen. The strain paths employed were the push-pull straining (Case 1) and the circular straining (Case 2) where von Mises' equivalent strain amplitude was increased by 0.05 % at each 10 cycles. In the figures, $\Delta\varepsilon_I$ and $\Delta\sigma_I$ are the maximum principal strain and stress ranges under non-proportional loading which can be calculated by ε, γ and σ, τ. The obtained result shows clearly that behaviors of the additional hardening due to non-proportional loading are different between SUS316 and SGV410. The degree of additional hardening of SUS316 was approximately twice than that of SGV410, whereas LCF life in Case 2 was decreased down to 1/5 in comparison with that in Case 1 for both steels as shown in Fig. 7. Therefore, the additional hardening and the reduction in failure life are closely related, which depends on
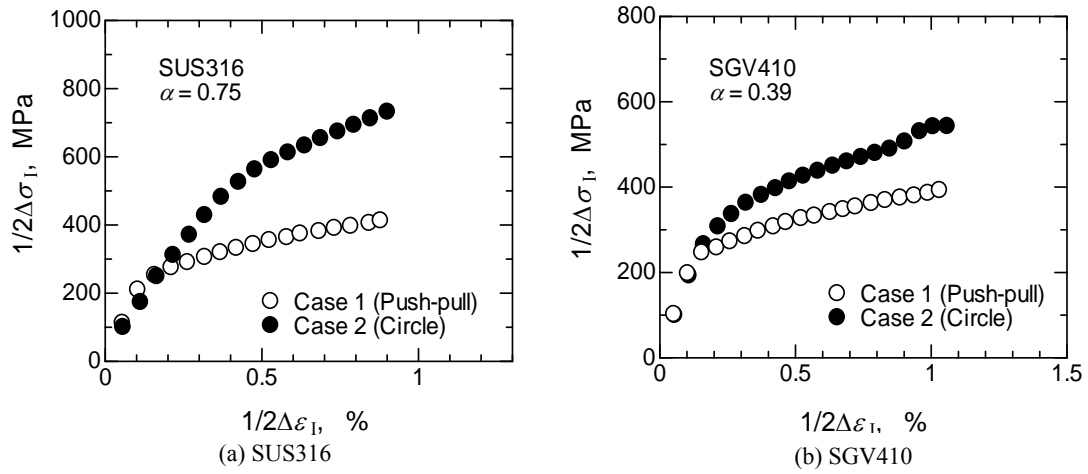
Fig. 8. Cyclic stress and strain relation obtained by multiple step-up test under push-pull and circular strainings.

material resulted from the difference in the deformation behavior due to crystal structural dependency [16,18,19].

Figs 9 (a) and (b) show N_f correlated by non-proportional strain range, $\Delta\varepsilon_{NP}$. α employed here is the material constant evaluated from the degree of additional hardening. For SUS316 (α=0.75) in Fig. 9 (a), N_f in Case 2 is almost the same as that in Case 1. On the other hand, N_f for SGV410 (α = 0.39) in Fig. 9 (b) is correlated unconservatively in Case 2. The similar trend also can be observed in other FCC and BCC materials which will be shown in the following section.
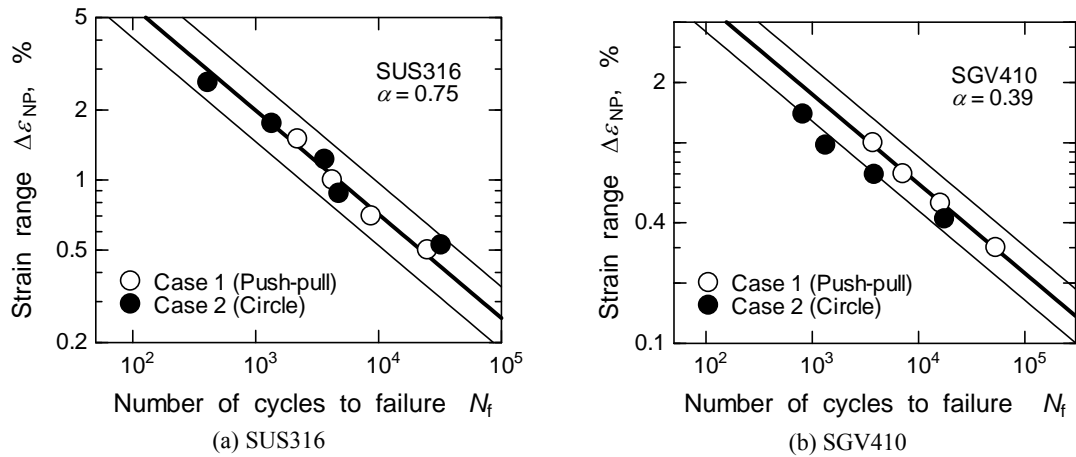

Fig. 9. Relationship between $\Delta\varepsilon_{NP}$ and N_f.

Fig. 10 shows the re-plot of relationship between $\Delta\varepsilon_{NP}$ and N_f for SGV410 by using α^* as material constant for evaluating the degree of reduction in failure life. The correlation in this figure shows N_f in Case 2 is plotted within the factor of 2 band with α^*=0.85. The value of α^* is slightly larger than that for SUS316 (α^*= α=0.75).
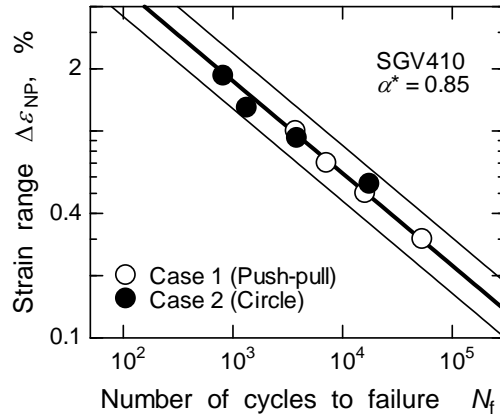
Fig. 10. Relationship between $\Delta\varepsilon_{NP}$ and N_f for SGV410 with α^*=0.85.

In order to investigate the relationship between multiaxial LCF life and cyclic hardening under non-proportional loading for 12 kinds of test materials. The relationship between α and α^* is discussed based on the experimental results. The universal slope method equated in Eq. (11) [20] was employed to obtain the life curves with a small number of data in Case 1 and Case 2 for each material. The equation is shown by,

$$\Delta\varepsilon_{NP} = \left(1 + \alpha^* f_{NP}\right) \Delta\varepsilon_I = A N_f^{-0.12} + B N_f^{-0.6} \tag{11}$$

where the coefficients A and B are equated as $3.5\sigma_B/E$ and $\varepsilon_f^{0.6}$ respectively, according to the definition of the universal slope method. Here, E, σ_B and ε_f are Yong's modulus, tension strength and elongation. In this study, A is put to $3.5\sigma_B/E$ but B and α^* are determined as life curves in Case 1 and Case 2 are corresponding at same $\Delta\varepsilon_I$ for each material.
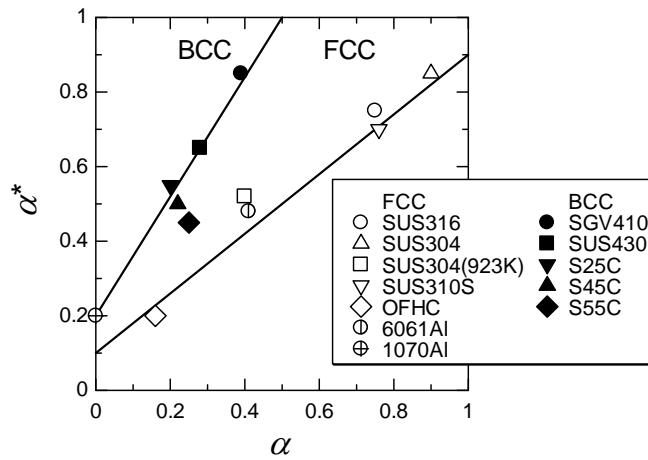

Fig. 11. Relationship between α and α^*.

Fig. 11 shows the relationship between α and α^* for each material. The open mark shows the data for FCC materials, the solid mark the data for BCC materials. The relationship is shown by two straight lines separately in FCC and BCC materials although a few data are scattered on the both sides of the band. The result in Fig. 11 shows that reduction in failure life has close relationship with additional hardening in non-proportional loading, which depends on crystal structure of tested materials. The relationship between α and α^* can be expressed experimentally as,

$$\alpha^* = \begin{cases} 0.8\alpha + 0.1 & \text{for} \quad \text{FCC} \\ 2\left(0.8\alpha + 0.1\right) & \text{for} \quad \text{BCC} \end{cases} \tag{12}$$

In order to verify the application of life evaluation under non-proportional loading, the comparison of N_f in Case 2 obtained from experiment evaluated by Eq. 11 based on life curve in push-pull test (Case 1) is shown in Fig. 12. In Eq. 11, α^* was used for material constant. In the figure, N_f^{exp} is the failure life in experiment and N_f^{cal} the failure life estimated by Eq. 11. All the data are correlated within the factor of 2 band. Consequently, the good correlation of lives in Fig. 12 suggests that failure life under non-proportional loading for various materials can be estimated by $\Delta\varepsilon_{NP}$ if the intensity of additional hardening is obtained from experiment.
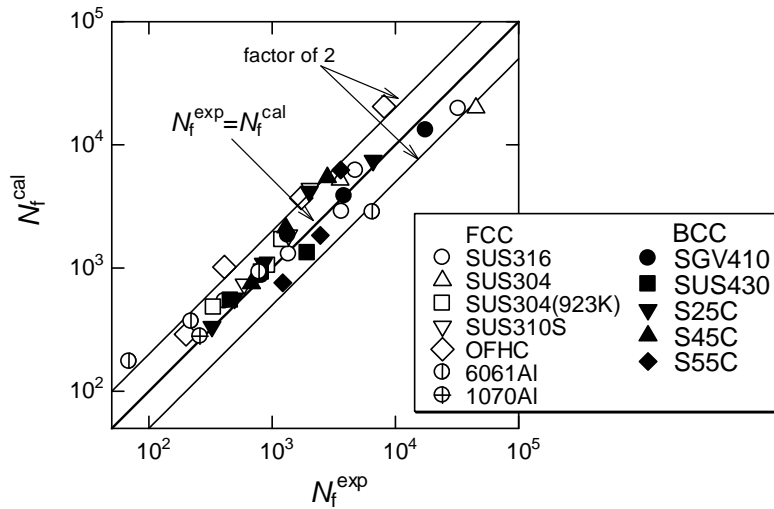

Fig. 12. Comparison of N_f in Case 2 between calculation and experiment.

A simple method for evaluation of α and life estimation

As discussed above, multiaxial LCF life shows the large reduction in failure life under non-proportional loading in comparison with that under proportional loading. By using non-proportional strain parameter, $\Delta\varepsilon_{NP}$ in Eqs 7 and 11, multiaxial LCF lives can be estimated from the data in push-pull loading test. However, to obtain the value of material constants, α and α^*, multiaxial fatigue tests under non-proportional loading are
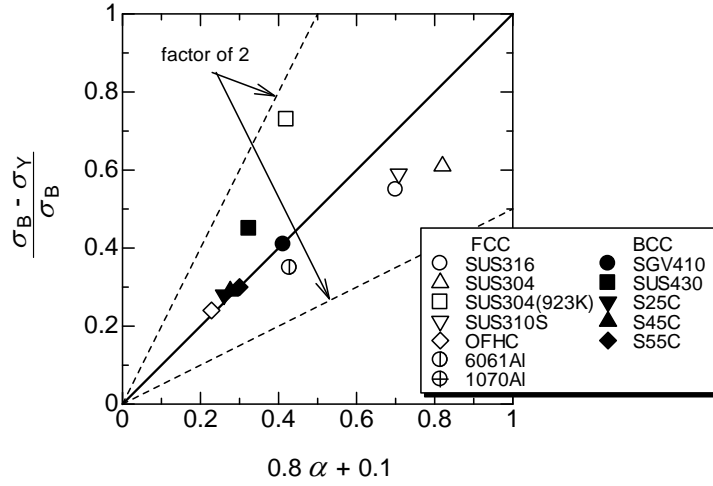
Fig. 13. Relationship between $(\sigma_B - \sigma_Y)/\sigma_B$ and α.

necessary, but it is usually difficult procedure. If α and α^* can be obtained without conducting the multiaxial fatigue test, it will be very convenient for engineers to estimate LCF life under non-proportional loading. This section discusses the reevaluation of α by focusing on the relationship between α and material constants obtained by the static tension test. Cyclic hardening and additional hardening behaviors should have close relationship with static deformation behavior, then a relationship between $(\sigma_B - \sigma_Y)/\sigma_B$ and α is shown in Fig. 13. Although some scatter of data is shown, the relationship can be equated approximately as,

$$0.8\alpha + 0.1 = \frac{\left(\sigma_B - \sigma_Y\right)}{\sigma_B} \tag{13}$$

where σ_B is tension strength and σ_Y yielding or 0.2% proof stress, According to Eqs 11–13, non-proportional strain range, $\Delta\varepsilon'_{NP}$, can be rewritten as,

$$\Delta\varepsilon'_{NP} = \left(1 + S \frac{\sigma_B - \sigma_Y}{\sigma_B} f_{NP}\right)\Delta\varepsilon_I = A N_f^{-0.12} + B N_f^{-0.6} \tag{14}$$

where coefficient S takes $S= 1$ for FCC materials and $S=2$ for BCC materials.

Fig. 14 shows the comparison of N_f in Case 2 between experiment and calculation. In the figure, N_f^{exp} is the failure life in experiment and N_f^{cal} the failure life estimated based on life curve in push-pull test (Case 1 test) by using $\Delta\varepsilon'_{NP}$ in Eq. (14). Consequently, all the data are correlated within a factor of 3 band and most of them correlated within the factor of 2 band. The good correlation in Fig. 14 suggests that multiaxial LCF life under non-proportional can be estimated by Eq. (14) with material constants obtained by the static tension test.
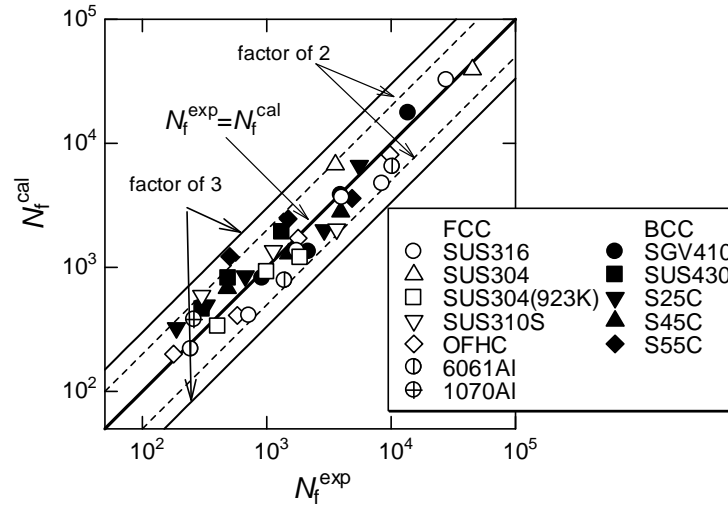
Fig. 14. Comparison of N_f in Case 2 between experiment and calculation by $\Delta\varepsilon'_{NP}$.

CONCLUSIONS

1. This paper showed a simple method of determining the principal stress and strain ranges together with the mean stress and strain under proportional and non-proportional loading in 3D stress and strain space. It also presented the method of defining the rotation and deviation angles of the maximum principal stress and strain.

2. The paper extend the non-proportional factor, f_{NP}, from 2D to 3D stress and strain space with the consistency with the previous definition of it in the 2D space.

3. Reduction in failure life has close relationship with additional hardening under non-proportional loading, which depends on crystal structure of tested materials.

4. The parameter α^* which relates to the degree of reduction in failure life is effective in life evaluation for various kinds of materials.

5. The relationship between α^* and α which relates to the additional hardening due to non-proportional loading is equated by linear relationships separately in BCC and FCC materials.

6. α is closely related with the behavior of static tension test and can be equated by $0.8\alpha + 0.1 = (\sigma_B - \sigma_Y)/\sigma_B$.

7. Failure life under non-proportional loading for various materials can be evaluated by $\Delta\varepsilon_{NP}$ if the intensity of additional hardening is obtained as equated by $\Delta\varepsilon_{NP}$ and $\Delta\varepsilon'_{NP}$.

REFERENCES

1. ASME, Boiler and Pressure Vessel Code Section III, Division 1 NH 2004.

2. ASME, Boiler and Pressure Vessel Code Section VIII, Division 3 2004.
3. Fatemi A, Socie DF, A critical plane approach to multiaxial fatigue damage including out-of-phase loading. *Fatigue Fract Eng Mater Struct*, 1988;11:149-165.
4. Nitta A, Ogata T, Kuwabara KJ, Fracture modes and fatigue life evaluation of SUS 304 stainless steel under non-proportional biaxial loading conditions. *J Society Material Science*, Japan, 1989;38:416-422.
5. Doong SH, Socie DF and Robertson IM, Dislocation substructure and non-proportional hardening, *J Engng Mater Technol*, 1990;112(4):456-564.
6. Itoh T, Sakane M, Ohnami M, Socie DF, Nonproportional low cycle fatigue criterion for type 304 stainless steel. *Trans ASME J Eng Mater Mater Technol*, 1995;117:285-292.
7. Itoh T, Nakata T, Sakane M, Ohnami M, Non-proportional low cycle fatigue of 6061 aluminum alloy under 14 strain path. *Multiaxial Fatigue and Fracture* (Macha *et al.*, eds.), 1999;ESIS-25:41-54.
8. Carpinter A., Brighenti R., Macha E. and Spagnoli A. Expected principal direction under multiaxial random loading. Part II: numerical simulation and experimental assessment trough the weight function method. *International Journal of Fatigue*, 1999;21:89-96.
9. Socie DF, Marquis G, eds, Multiaxial Fatigue, SAE International, 2000.
10. Reis L., Li B. and Freitas M. Crack initiation and growth path under multiaxial fatigue loading in structural steels. *International Journal of Fatigue*, 2009;31:1660-1668.
11. Smith RN, Watson P, Topper TH, A stress-strain parameter for the fatigue of metals, *J Materials*, 1970;5(4):767-778.
12. Shamsaei N, Fatemi A, Socie DF, Multiaxial fatigue evaluation using discrimination stain paths, *Int J Fatigue*, 2011;33:597-609.
13. Itoh T, Effect of direction change in maximum principal strain axis on multiaxial low cycle fatigue life of type 304 stainless steel at elevated temperature, *J Society Material Science*, Japan, 2003;49:988-993. [in Japanese]
14. Itoh T, A model for evaluation of low cycle fatigue lives under non-proportional straining, *J Society Material Science*, Japan, 2001;50(2):1317-1322. [in Japanese]
15. Itoh T, Miyazaki T, A damage model for estimating low cycle fatigue lives under nonproportional multiaxial loading, *Biaxial/Multiaxial Fatigue & Fracture* (Carpinteri *et al.*, eds.), 2003; ESIS-31:423-439.
16. Itoh T, Yang T, Material dependence of multiaxial low cycle fatigue lives under non-proportional loading, *Int J Fatigue*, 2011;33:1025-1031.
17. Wang C.H. and Brown M.W. A path-independent parameter for fatigue under proportional and non-proportional loading. *Fatigue & Fracture of Engineering Materials & Structures*, 1993;16(12):1285-1298.
18. Doong S.H. and Socie D.F. Constitutive modeling of metals under non-proportional cyclic loading. Transaction of the American Society of Mechanical Engineers, *Journal of Engineering Materials and Technology*, 1991;113(1):23-30.
19. Itoh T., Sakane M., Ohnami M. and Ameyama K. Effect of stacking fault energy on cyclic constitutive relation under non-proportional loading, *Journal of the Society of Materials Science*, Japan, 1992;41(468):1361-1367 [in Japanese].
20. Manson S.S. Fatigue, a complex subject: some simple approximations, Exp. Mech. (1965);5:193-226.